15th World Congress on Computational Mechanics (WCCM-XV)
8th Asian Pacific Congress on Computational Mechanics (APCOM-VIII)
Virtual Congress: 31 July – 5 August 2022
S. Koshizuka (Ed.)

AERODYNAMIC AND ACOUSTIC DESIGN OPTIMIZATION OF A MULTIPLE PROPELLER COMBINATION FOR DISTRIBUTED ELECTRICAL PROPULSION

ANTONIO VISINGARDI[1], MATTIA BARBARINO[2] AND DOMENICO QUAGLIARELLA[3]

[1]Centro Italiano Ricerche Aerospaziali
Via Maiorise – 81043 Capua (CE) - Italy
E-mail: a.visingardi@cira.it – URL: www.cira.it

[2] Centro Italiano Ricerche Aerospaziali Postal Address
Via Maiorise – 81043 Capua (CE) - Italy
E-mail: m.barbarino@cira.it – URL: www.cira.it

[3] Centro Italiano Ricerche Aerospaziali
Via Maiorise – 81043 Capua (CE) - Italy
E-mail: d.quagliarella@cira.it – URL: www.cira.it

Key words: Distributed Electric Propulsion, Aeroacoustics, Multi-Objective Optimization, Boundary Element Method, Ffwocs-William & Hawkings equation, Genetic Algorithms

Abstract. *This manuscript illustrates an optimization procedure carried out on a large-scale wind tunnel model conceived to investigate the aerodynamic and acoustic performance of a Distributed Electric Propulsion (DEP) system installed on the wings of a regional aircraft in high lift conditions. The aim of the optimization process is to obtain the best possible improvements in terms of noise and aerodynamic performance by modifying the propellers' layout of the Wing + DEP wind tunnel model. A multi-objective, multi-point design approach is adopted based on evolutionary computing. The research work is carried out in the framework of the VENUS EU-funded project GA-886019.*

1 INTRODUCTION

Driven by economic and ecological requirements, the aeronautical community is continuously investing in the reduction of fuel consumption and CO2 emissions of currently operating and new aircraft. Despite strong effects concerning reducing fuel consumption can be made with regards to jet engine improvement, the awareness of the need for a disruptive advancement in propulsion technologies is nowadays more and more diffused in the research community, not only for the potential global hazards associated with emissions produced by traditional aircraft propulsion systems, but also for the ever more limited supply of traditional petroleum fuel sources.

Following national and international laws and agreements between countries, civil aircraft manufacturers and airliners have to realize an explicit reduction of airplane fuel consumption until the year of 2020. For this purpose, many activities are recently exploring solutions to

improve in a short term the propulsive efficiency of currently flying technologies (turboprop/ fan). However, this cannot represent a long-term solution, where even advanced conventional designs cannot cope with the target performance set out in [1] and [2] in terms of both energetic efficiency and emissions.

One of the propulsion configurations that is believed to meet these challenging goals is the so-called Distributed Electric Propulsion (DEP), that on one hand exploits the benefits of electric engines to drastically reduce (global) fuel consumption and emissions and on the other hand takes benefit from the distribution on the aircraft of multiple small propulsors, with different locations with respect to the wing and different types of the propulsors themselves (jet, fan, propeller).

Due to the tight integration of the propulsion system into the wing-body surfaces of the aircraft, the major benefit gained from the adoption of DEP is mainly aerodynamic; the propellers are used to produce the required thrust and, at the same time, to increase the dynamic pressure of the flow and the effective angle of attack of the wing, thus increasing the wing lift.

Nevertheless, DEP propellers have to be carefully designed because, even if electric motors are scalable and do not lose efficiency when size is reduced, they lose efficiency when their diameter is reduced. Therefore, the propeller diameter must be carefully selected to obtain the best benefits. For this reason, DEP is usually conceived to be activated only during the take-off/landing phase to increase lift coefficient and therefore allow the design of a wing with a smaller surface and, therefore, with a smaller weight. In addition, the increase in the number of propellers can potentially penalize the aeroacoustics of these new configurations. Thus, a careful aerodynamic and acoustic design of this new aircraft must be pursued.

The European research project VENUS (inVestigation of distributEd propulsion Noise and its mitigation through wind tUnnel experiments and numerical Simulations) [3] is an H2020 / CleanSky JU thematic topic with the objective to understand the physics behind the aeroacoustics of the Distributed Electric Propulsion (DEP), set-up numerical procedure for DEP noise assessment, and produce an experimental data-set to be used both as experimental DEP noise validation reference and for providing support to the identification of the main parameters affecting DEP noise.

In this framework, a specific activity was dedicated to the performance of aerodynamic and aeroacoustic analyses of three propellers considering the interaction with wing and high-lift devices.

This manuscript describes the optimization procedure built up with the aim to obtain the best possible improvements in noise and aerodynamic performance of a Multiple Propeller Combination by modifying the propellers' layout of the Wing-DEP wind tunnel model. The outcomes of this optimization procedure are illustrated and discussed in detail.

2 NUMERICAL TOOLS FOR THE AERODYNAMIC & AEROACOUSTIC DESIGN OF THE MULTIPLE PROPELLER COMBINATIONS

The aerodynamic and aeroacoustic design activity of the multiple propeller combinations was carried out by setting up a multi-objective optimization procedure which, by the use of a suitable medium-fidelity aerodynamic solver and an aeroacoustic solver based on the FW-H formulation, investigated several different layouts of the VENUS wind tunnel model with the aim to identify solutions providing low-noise and high-aerodynamic performance when

compared to a baseline configuration. The VENUS wind tunnel model consists of a flapped wing segment and three propellers installed ahead of the wing. The term layout used in the following specifically refers to the mutual position of the three propellers and their position with respect to the wing geometry.

2.1 The aerodynamic solver

The aerodynamic simulations were carried out using the medium-fidelity code RAMSYS [4], an unsteady, inviscid, and incompressible free-wake vortex lattice boundary element methodology (BEM) solver for multi-rotor, multi-body configurations developed at CIRA. It is based on Morino's boundary integral formulation [5] for the solution of Laplace's equation for the velocity potential φ. The surface pressure distributions are evaluated by applying the unsteady version of Bernoulli's equation, which is then integrated to provide the forces and moments on the whole configuration and its components. A computational acceleration is obtained by applying the parallel execution via the OpenMP Application Programme Interface.

2.2 The acoustic solver

The aeroacoustic simulations were carried out by using the aerodynamic database evaluated by RAMSYS [4] consisting of the rotor blade pressure distributions, and by applying the OptydB FW-H solver based on FW-H formulation [6] and [7]. The advanced-time formulation of Farassat 1A is employed, and the linear terms (the so-called thickness and loading noise contributions) are computed through integrals both on the moving blades surface (impermeable/rigid surface formulation) and on the fixed surfaces. The quadrupole contribution, due to the nonlinear terms distributed in the perturbed field around the blade, is neglected.

2.3 Optimization tools

The software used to solve the design optimization problem is the ADGLIB library (ADaptive Genetic algorithm LIBrary) [8]. It is an in-house evolutionary optimization software library based on the hybridization concept. ADGLIB allows to easily define evolutionary optimization algorithms that combine, for example, classical bit-string-based genetic algorithms with hill-climbing specialized operators. The choice is motivated by the need to improve the efficiency of genetic algorithms while keeping their flexibility in searching large design spaces. The specific implementation allows using the genetic algorithm hybridized either with gradient-based operators, like BFGS [9], or other sophisticated evolutionary algorithms like CMA-ES. These operators can also be used stand-alone for a plain gradient-based or CMA-ES optimization run. ADGLIB is fully parallel at the level of population evaluation. Only two of the available optimization algorithms in the library were used in the VENUS optimization activity, namely a classical Multi-Objective Genetic Algorithm (GA) [10] and [11] and the Covariance Matrix Adaptation Evolution Strategy (CMA-ES) [12].

3 SET-UP OF THE WIND TUNNEL MODEL & TEST CONDITIONS

3.1 Propeller and wing geometries

The propeller, named E1357, was specifically designed by CIRA [12] to maximize the

aerodynamic performance for DEP applications and minimize its acoustic signature. The blade plan form is shown in **Figure 1**. The wing of the wind tunnel model consists of a rectangular segment generated by a NACA 63-(2)-415 airfoil modified to house a slotted flap, as shown in **Figure 2**.

3.2 Set-up of the wind tunnel model

The attitude of the wind tunnel model was set equal to α=5 deg for both take-off and landing flight conditions. In the first case, the slotted flap was deflected of an amount of δ=20 deg, whereas a deflection of δ=35 deg was chosen for the second case.

The three propellers were co-rotating and counter-clockwise when looking at the wing from the leading edge toward the trailing edge, **Figure 3**.

The simple installation of the three propellers ahead of the wing leading edge produced an increase of about 9% in their thrust coefficient, as it is shown in **Table 1** and **Table 2**. Therefore, in order to perform the optimization activity at the nominal design thrust coefficient of the propellers (CT=0.072), it was necessary to trim each propeller by modifying the collective blade pitch. This pitch adjustment was only applied to the baseline configuration of the wind tunnel model in take-off flight conditions, thus implying that different values of the propeller thrust coefficient would be obtained in all the other test conditions. The new pitch of the blades and the resulting performance of the three propellers are illustrated in **Table 3**, which highlights an average reduction in pitch of about 0.5 deg.

Table 1: Installed propellers - Performance at assigned collective pitch

AoA = 16.42 deg	CT	CQ inv.	ETA inv.
Propeller Left	0.07867	0.01874	0.8398
Propeller Centre	0.07869	0.01873	0.8405
Propeller Right	0.07823	0.01863	0.8400

Table 2: Installed propellers - CT & Collective pitch variations [deg]

AoA = 16.42 deg	Δ CT %	Δ AoA [deg]
Propeller Left	9.23	0.594
Propeller Centre	9.26	0.598
Propeller Right	8.73	0.550

Table 3: Installed propellers - Performance at nominal CT

CT = 0.072	AoA [deg]	CT	CQ inv.	ETA inv.
Propeller Left	15.826	0.07202	0.01708	0.8433
Propeller Centre	15.822	0.07203	0.01707	0.8438
Propeller Right	15.870	0.07195	0.01709	0.8420

The wind tunnel model consists of a rectangular wing ending with two end-plates, installed to reduce the 3D tip effects, and located at a height from the floor equal 1.5 meters. Each of the three propellers is installed on a nacelle, and their hubs are covered with a spinner having a streamlined shape. Nevertheless, in order to expedite the optimization process, a set of simplifications were made for the numerical simulations. In particular:

- the end plates at the wing tips were not modelled;
- the ground effect, small but however not absent, was not considered;
- no hub nor nacelle geometries were modelled.

3.3 Wind tunnel model space and time discretization

Each of the twelve blades was discretized by using 40 chordwise x 14 spanwise panels, whereas the wing was discretized by 78 chordwise x 13 spanwise panels. Four propeller revolutions were required to reach a converged solution of the average thrust coefficients. The wake was modelled considering four spirals. **Figure 4** shows the propeller layout in baseline configuration and the wake developing from both the propeller blades and the wing as a result of the numerical simulations.

The whole optimization procedure consisted of two main phases:

- MOO execution and selection of representative results;
- verification of the representative results by performing simulations at a higher time resolution.

In the first phase, a time step corresponding to an azimuth step of 15 deg was adopted, whereas the verification analyses at high-resolution were carried out at an azimuth step of 3 deg. This solution was motivated by the fact that high resolution aerodynamic analyses required about 5.5 hours of elapsed time in OpenMP mode using 16 cores per single run, thus requiring about 11 hours for the analysis of a single individual. The same calculation in coarser time resolution required about 36 minutes of elapsed time per individual.

A preliminary analysis was carried out in order to assess the feasibility of this solution by comparing the results in terms of the thrust coefficient time history. **Figure 5** shows the unsteady component of the thrust coefficient using the coarse discretization (15 deg) and the fine discretization (3 deg). The two solutions are in a satisfactory agreement with only a slight difference in capturing the four peaks. A measure of the unsteadiness of the phenomenology was expressed in terms of the RMS of the fluctuation, which turned out to be extremely low (order of magnitude 10-5).

3.4 Wind tunnel model parameters

The wind tunnel model parameters selected for the layout optimization activity are illustrated in **Table 4**

Table 4: Wind tunnel model parameters

Parameter	Value	Parameter	Value
Propeller diameter D [m]	0.556	D/C	0.87
Propeller speed Ω [RPM]	6840	Wind tunnel speed V [m/s]	40.00
Wing span B [m]	2.50	T [N] (per propeller)	109.50
Wing chord C[m]	0.635	CT (per propeller)	0.072

4 MICROPHONE ARRAYS

The numerical analysis of the noise generated by the wind tunnel model in the two flight conditions and in the different layout configurations was carried out by considering 159 microphones organized in three circular arrays located in the Pininfarina wind tunnel plenum chamber:

- X array: installed at the outlet of the WT convergent duct;
- Y array: installed on the side wall at the WT model portside at a height from the floor equal to 1.7 m;
- Z array: installed on the ceiling of the plenum chamber.

The offsets of the circular arrays centre are shown in **Table 5**

Table 5: Microphone arrays – Centre offsets

Array	Offset X [m]	Offset Y [m]	Offset Z [m]
X	0.050	0.000	3.719
Y	3.675	-4.200	0.000
Z	3.175	0.000	4.000

referred to a frame of reference having its origin at the outlet of the WT convergent duct. In particular:

- X=0 at the outlet of the WT convergent duct
- Y=0 at the centre of the WT test chamber
- Z=0 at the floor

Nevertheless, the numerical simulations made use of a different frame of reference having its origin in the point obtained by the intersection between the wing quarter chord line and the wing mid span plane and corresponding to the balance reference centre. This implied a shift in the direction of the arrays centre offsets equal to Xshift = -3.675 m.

Figure 6 illustrates a view of the wind tunnel flow region. The width (Y) and the height (Z) are those of the plenum chamber, and are equal to 9.6 m and 4.2 m, respectively. The length (X) is the one of the jet-flow, equal to 8 m, and starting from the outlet of the convergent duct.

5 OPTIMIZATION PROCEDURE

An optimization procedure was built up with the aim to obtain the best possible improvements in noise and aerodynamic performance of a Multiple Propeller Combination by modifying the propellers' layout of the Wing-DEP wind tunnel model.

A multi-objective optimization was carried out in two main steps by the application of:

- a preliminary coarse-grained multi-objective Pareto front exploration;
- a sequence of constrained single-objective optimizations focused on representative areas of the Pareto front case by case alternatively selecting as objective functions the Overall Sound Pressure Level (OASPL) or the wing lift coefficient CFz.

The optimization was two-point and referred to the Take-off & Landing flight conditions.

More specifically, the optimization consisted of a sequence of computations using different evolutionary optimization algorithms to investigate as wide as possible the design space:

- classical multi-objective Genetic Algorithms: for the preliminary multi-objective exploration;
- Covariance Matrix Adaptation Evolution Strategy (CMA-ES): to explore specific Pareto front areas in-depth.

A total amount of about 8000 two-point individuals were analysed, summing up to almost

16000 numerical simulations.

5.1 Design parameters

Four design parameters were identified for the optimization of the wind tunnel model layout, **Figure 7**. Four coordinates of each propeller's hub centre were selected as a first set of design parameters. In particular, the X coordinates of the outer propellers, XhubO, were jointly changed independently of the X coordinate of the central propeller, XhubC, the Y coordinates of the outer propellers, YhubO, were symmetrically changed with respect to the central propeller whose coordinate was kept as fixed and located at the wing mid-span, YhubC = 0, the Z coordinates of the three propellers, Zhub, were jointly changed.

A fifth parameter, $\Delta\Psi$, was additionally considered in order to investigate the effect of de-phasing the central propeller azimuth position with respect to the outer propellers, which were always kept in-phase and with an initial value $\Delta\Psi$=0 deg.

Table 6 summarizes the hub coordinates and the initial phase of the three propellers for the baseline configuration. The coordinates are referred to the wind tunnel model frame of reference having origin in the red bullet of **Figure 8** corresponding to the intersection between the wing quarter chord line and the wing mid span plane.

Table 7 and **Figure 8** show the ranges of variation of the design parameters that were indicated by IBK, on the basis of structural requirements and mechanical complexity of the wind tunnel model, and agreed by the VENUS consortium.

Table 6: Settings for the baseline configuration

	Propeller		
	Left	**Centre**	**Right**
Xhub [m]	-0.44875	-0.44875	-0.44875
Yhub [m]	-0.58380	0.00000	0.58380
Zhub [m]	0.00000	0.00000	0.00000
Phase [deg]	0.00	0.00	0.00

Table 7: Ranges of the design parameters

	Boundary	
	Lower	**Upper**
Xhub [m]	-0.50875	-0.38875
|Y|hub [m]	-0.54200	-0.69400
Zhub [m]	-0.10000	0.10000
Phase [deg]	0.00	90.00

5.2 Design functions

The outcomes of the optimization activity were monitored and evaluated in terms of five design functions.

In particular, two objective functions were defined:

1. OASPLavg: the average of the Overall Sound Pressure Level evaluated on the 159 microphones composing the three arrays X, Y, Z installed in the Pininfarina wind tunnel;
2. CFz: the wing lift coefficient, evaluated as the lift produced by the portion of the wing corresponding to the outmost position of the axes of rotation of the outer propellers, namely YhubO ϵ [-0.694; +0.694] m, non-dimensionalised with respect to wind tunnel dynamic pressure and the wing area;

and three additional design functions:

3. CFz/CMy: the ratio between the wing lift and pitching moment coefficients;
4. Eff (η): the inviscid component of the average efficiency of the three propellers;
5. CT: the average thrust coefficient of the three propellers.

In order to ease the analysis of the two-point optimization results, it was decided to ultimately investigate and represent the average of the design functions obtained in take-off and landing:

$$DF_{avg} = \frac{DF_{TO} + DF_{LA}}{2} \quad (1)$$

This choice was made possible thanks to the same behaviour observed in each of the five design functions for the two flight conditions.

Additional variables were also evaluated during the simulations and fully reported in the obtained databases:

1. CQ: the average torque coefficient of the three propellers;
2. CMy: the wing pitching moment coefficient;
3. OASPLavg-A: the average of the A-weighted Overall Sound Pressure Level evaluated on the 159 microphones.

5.3 Optimization flowchart

The flowchart of the optimization procedure is illustrated in **Figure 9**. Its structure is simple and linear: The design parameters represent the input data; the optimization activates, in parallel, the two branches of the Take-off and Landing flight conditions. Four penalty functions are then defined to constrain the selection of suitable solutions. These are the design parameters and one of the two objective functions that, during the whole optimization process, have been considered objective functions or constraints depending on the region of the design space requiring a more in-depth investigation. The main objective function is represented by the noise reduction expressed in terms of OASPL.

6 ANALYSIS OF THE RESULTS

6.1 Multi-objective optimization (MOO)

The whole optimization procedure consisted of a number of different optimization strategies in order to investigate the design space as widely as possible. **Figure 10** shows the complete set of MOO results in the plane OASPLavg vs CFzavg. The different colours indicate a different degree of fulfilment of the constraints of the five design functions, and the blue circles, in particular, represent those solutions fulfilling all constraints. The MOO results show two separate clouds of points. The one at higher OASPLavg is the result of the optimization during which the de-phasing of the central propeller was not activated. It can be observed that the improvement obtained with respect to the baseline configuration (red square) were null in terms of noise reduction and negligible in terms of increase in the wing lift (green triangle). Starting from this solution, the search for the best phase azimuth angle of the central propeller was activated. The whole process corresponds in **Figure 10** to the points located at about CFzavg = 0.78 and shows a progressive reduction in noise until reaching the lowest noise value corresponding to the point represented by the blue triangle. **Figure 11** shows, in particular, the results of this optimization subset and indicates a sinusoidal behaviour with the best de-phasing

obtained for a value of 35 deg. Staring from the blue triangle point, three more optimization subsets were carried out: two aimed at improving the aerodynamic performance (magenta and cyan triangles) the third aimed at improving the noise performance (orange triangle).

Four Pareto fronts were extracted from the MOO results. **Figure 12** illustrates the 2D Pareto front, shown in red line and consisting of 46 points, and three 3D Pareto fronts, each consisting of about 290 points, with the third design function corresponding to the propellers' efficiency EFFavg, the wing lift-to-pitching moment ratio CFz/CMyavg, the propellers' thrust coefficient CTavg, respectively. Four Pareto front points were then selected and represented in **Figure 12** as red, green, blue and cyan big circles.

6.2 High-resolution analysis of selected representative points

The MOO procedure allowed the identification of hundreds of points, in principle representing an improvement with respect to the baseline configuration. In order to confirm the results obtained, high-resolution analyses were carried out with the azimuth step of 3 deg for ten representative points:

- Baseline configuration
- Optimal point at Phase 0 deg
- Optimal point at Phase 35 deg
- Two Best Aerodynamic points
- Best Noise point
- Three points of the 2D Pareto
- One point of the 3D Pareto front Efficiency

Figure 13 illustrates the results in high resolution relative to these ten representative points. Starting from the baseline configuration, improvements in the design functions were always obtained, except for the ratio CFz/CMyavg for which only the solutions on the Pareto front red and green circles represented an improvement. **Table 8** shows the changes in the performance of the different layouts in terms of the variation of the design functions with respect to the baseline configuration. In particular: a reduction of almost 3dB was obtained for the Pareto Front 3 configuration; an increase of more than 2% was obtained in the wing lift of Pareto Front 1; Improvements of almost 1.5% in CFz/CMy ratio and efficiency and an increase of about 6% for the thrust coefficient were obtained for the Pareto Front 4 configuration.

Table 8: Design functions percentage improvements

	OASPL [dB]	CFz [%]	CFz/CMy| [%]	EFF [%]	CT [%]
Baseline	0.00	0.000	0.000	0.000	0.000
Opt. Phi = 0 deg	-0.03	0.547	0.013	0.093	0.314
Opt. Phi = 35 deg	-2.67	0.339	0.083	0.071	0.294
Best Aero 1	-2.67	1.490	0.203	0.171	0.510
Best Aero 2	-2.67	1.460	0.017	0.014	0.135
Best Noise	-2.74	1.154	0.602	0.329	1.098
Pareto F. 1	-2.17	2.243	0.606	0.864	3.481
Pareto F. 2	-2.49	2.134	0.441	0.576	2.511
Pareto F. 3	-2.84	0.613	0.309	0.045	0.088
Pareto F. 4	-2.04	1.209	1.345	1.406	5.891

6.3 Optimized layouts

The optimized layouts of the ten representative points are illustrated in the following.

Figure 14 shows the chordwise location (X direction) of the central propeller disk plane with

respect to the one of the outer propellers. Starting from the common position in the baseline configuration, the majority of the new layouts show a tendency for the disk planes to be staggered one over the others. The only exception is represented by the two solutions maximizing the efficiency, Pareto Front 4, and minimizing the noise, orange triangle, respectively, where the three propellers tend to remain in the same plane.

The x-axis of **Figure 15** shows the nondimensional spanwise position of the outer propellers with respect to the central one, which was kept fixed during the optimization. The figure indicates that the three propellers tend to move closer to each other in all the optimised layouts. In some particular cases, such as for the points lying on the 2D Pareto front, the best solution is represented by the outer propellers being overlapped with the central one. This solution was made possible by the chordwise staggering of the three propellers and by the de-phasing of the central one.

The y-axis of **Figure 15** shows the vertical position of the three propellers for the various new layouts. In all cases, the propellers tend to lie in the wing plane or on the lower side of it. No solution was found with the propellers located on the upper side of the wing plane.

The top and front views of some new layouts are shown in **Figure 16**. The staggered positions of the disk planes and the overlapping propellers can be easily observed.

6.4 Acoustic results

The acoustic results were represented in terms of OASPLavg contour maps for the three arrays of microphones (array X; Y; Z) in both take-off and landing flight conditions.

Figure 17 shows the take-off and landing flight conditions results for three selected points. In all the cases, the noise on the array X increases spanning from the right bottom side to the left top side of the array, as shown by the red arrow, and the directivity remains almost constant. A significant noise reduction is obtained as soon as the 35 deg de-phasing of the central propeller is activated. Another peculiarity is represented by the Pareto front points, where a considerable reduction in the noise gradients can be observed. A similar general behaviour can be observed for the results in landing conditions with only a slight increase in the noise values.

On the array Y, in the baseline configuration, the noise shows an increase from far to the region where the propellers are located, with an inclined directivity shown by the red arrow. Starting from the 35 deg de-phasing activation, a radical change in both intensity and directivity is produced. In particular, the noise shows the tendency to increase from the WT model region outward, with a directivity almost orthogonal to the wing plane but with much milder noise gradients. Only slight differences in noise intensity can be observed between take-off and landing flight conditions.

Finally, the analysis of the noise distributions on the microphone array Z shows that on the baseline configuration the noise peak is mainly concentrated on the left span of the WT model, whereas milder values of the noise characterise the right span. The 35 deg de-phasing of the central propeller produces a radical change in noise distribution directivity with a shift of the noise peak toward the right-span wing tip. This is mainly due to the composition of the acoustic signals, with different phases, generated by the de-phased propellers. The wing left span region remains a region of relatively high noise intensity, surrounded by a low noise region. As a result, the left side region of the array Z is characterised by low noise and the right side by a high noise distribution producing a region of noise local minima about the wing mid-span. The behaviour

in the other test conditions remains unaltered from the qualitative standpoint. Slight differences in noise intensity can be observed between take-off and landing flight conditions.

12 CONCLUSIONS

The main outcome of this activity was represented by the 35 deg de-phasing of the central propeller, which turned out to be the most powerful means for noise reduction. No other means proved to be equally effective. The optimization always produced improvements for the optimization functions except for Cfz/CMyavg, which, in some cases, produced a performance downgrade. Reductions up to almost 3 dB were obtained for the OASPLavg; an improvement greater than 2% was obtained for the CFzavg and greater than 1.3% for CFz/CMyavg and EFFavg. The CTavg was improved up to almost 6%.

The optimized layouts showed several common trends. In particular, it was observed that:

- the best solutions were found by staggering and moving away, as much as possible, the outer propeller disks with respect to the central one. However, the opposite behaviour was found when searching for the maximization of the propellers' efficiency or the minimization of the noise;
- the close proximity or even the overlap of the propeller disks showed to be effective in improving both the aerodynamic and acoustic performance. Indeed, three solutions lying on the 2D Pareto front displayed such a behaviour;

in all the cases, the propellers' hub centers were found to be located below the wing plane.

From a purely acoustic standpoint, the 35 deg de-phasing of the central propeller produced different changes in noise intensity and directivity depending on the location of the microphone arrays. In particular:

- Array X: Noise increased from the right bottom to the left top side of the WT. The noise distribution showed the tendency to be uniform;
- Array Y: For in-phase propellers, the noise increased from far to close to the propeller's location with an inclined directivity. For de-phased propellers, the noise increased from close to far from the wing plane with an almost orthogonal directivity;
- Array Z: The de-phasing shifted the noise peak from about the center to the right of the array disk.

ACKNOWLEDGMENTS

This work is part of the project VENUS (inVestigation of distributEd propulsion Noise and its mitigation through wind tUnnel experiments and numerical Simulations), which has received funding from the Clean Sky 2 Joint Undertaking under the European Union's Horizon 2020 research and innovation program under grant agreement 886019.

REFERENCES

[1] Paris Agreement: COP21/CMPP11. At COP 21 in Paris, on 12-12-2015, Parties to the UNFCCC reached a landmark agreement to combat climate change and to accelerate and intensify the actions and investments needed for a sustainable low carbon future.

[2] Flightpath 2050 document: https://ec.europa.eu/transport/sites/transport/files/modes/air/doc/flightpath2050.pdf.

[3] Camussi, R., *VENUS*, project proposal submitted to the call H2020-CS2-CFP10-2019-

01, Aug 2019.

[4] Visingardi, A., D'Alascio, A., Pagano, A., Renzoni, P., *Validation of CIRA's Rotorcraft Aerodynamic Modelling SYStem with DNW Experimental Data*, 22nd European Rotorcraft Forum, Brighton, UK, 1996.

[5] Morino, L., *A General Theory of Unsteady Compressible Potential Aerodynamics*, NASA CR-2464, 1974.

[6] Casalino, D., Barbarino, M., Visingardi, A., *Simulation of Helicopter Community Noise in Complex Urban Geometry*, AIAA Journal, Vol. 49, No. 8 (2011), pp. 1614-1624. DOI: 10.2514/1.J05077.

[7] Casalino, D., *An advanced time approach for acoustic analogy predictions*, Journal of Sound and Vibration, 2003

[8] Quagliarella, D., *Aerodynamic Shape Design Using Evolutionary Computation: A Tutorial with Examples and Case Studies*, pages 529–581. American Institute of Aeronautics and Astronautics (AIAA), 2014.

[9] Nocedal, J., and Wright, S., *Numerical Optimization* (Chapter 6), Springer, 2nd edition, 2006.

[10] Vicini, A., Quagliarella, D., *Inverse and direct airfoil design using a multi-objective genetic algorithm*, AIAA journal, 35(9):1499–1505, 1997.

[11] Vicini, A., Quagliarella, D., *Airfoil and wing design through hybrid optimization strategies*, AIAA journal, 37(5):634–641, 1999;

[12] Hansen, N. *The CMA evolution strategy: A comparing review*, in Jose A. Lozano, Pedro Larrañaga, Iñaki Inza, and Endika Bengoetxea, editors, Towards a New Evolutionary Computation: Advances in the Estimation of Distribution Algorithms, pages 75–102. Springer Berlin Heidelberg, Berlin, Heidelberg, 2006. ISBN 978-3-540-32494-2. doi: 10.1007/3-540-32494-1_4. URL http://dx.doi.org/10.1007/3-540-32494-1_4;

[13] Pagano, A., *Aeroacoustic design of the isolated propeller*, Doc. N. CIRA-DTS-21-0660, Mar. 2021.

Figure 1: Propeller blade plan form

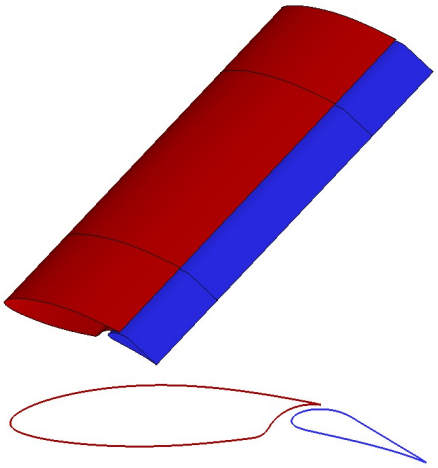

Figure 2: Wing geometry with the real slotted flap

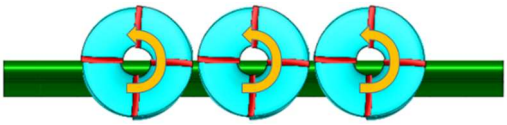

Figure 3: Propellers' sense of rotation

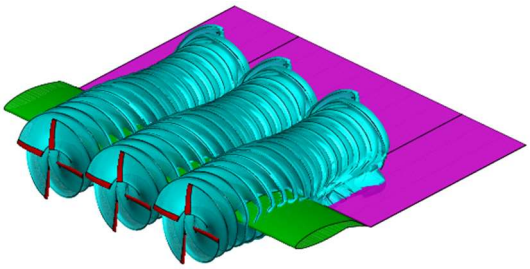

Figure 4: Wind Tunnel model geometry and relative wake development

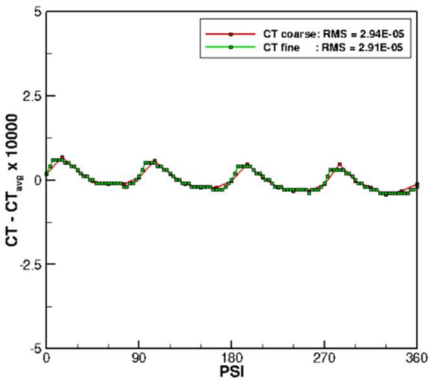

Figure 5: Coarsening of the time discretization

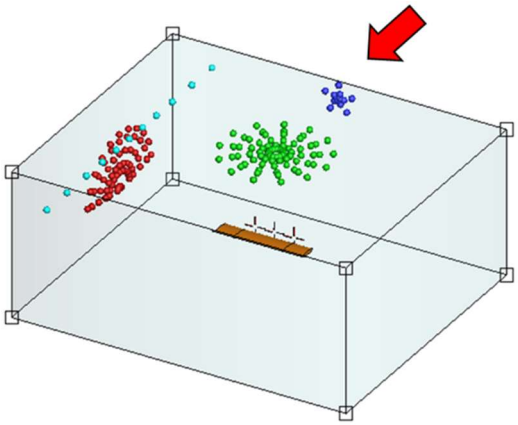

Figure 6: Microphone arrays in Pininfarina wind tunnel and wind tunnel model geometry

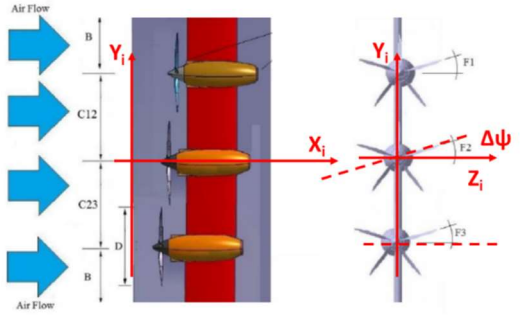

Figure 7: Sketch of wind tunnel model configuration and design parameters

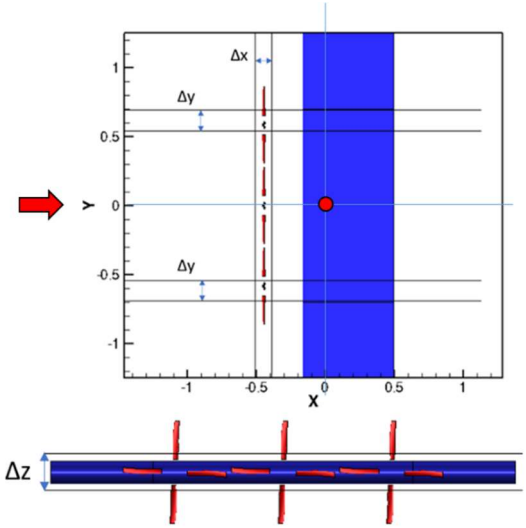

Figure 8: Ranges of the design parameters

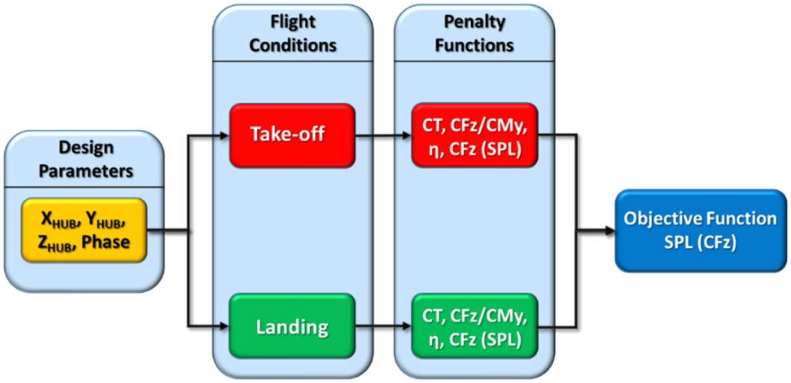

Figure 9: MOO flowchart

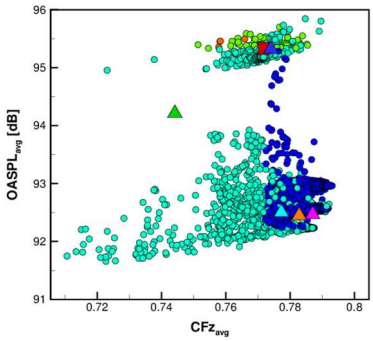

Figure 10: MOO results

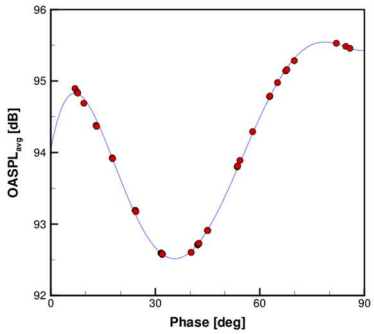

Figure 11: Effect of central propeller de-phasing on the OASPLavg objective function

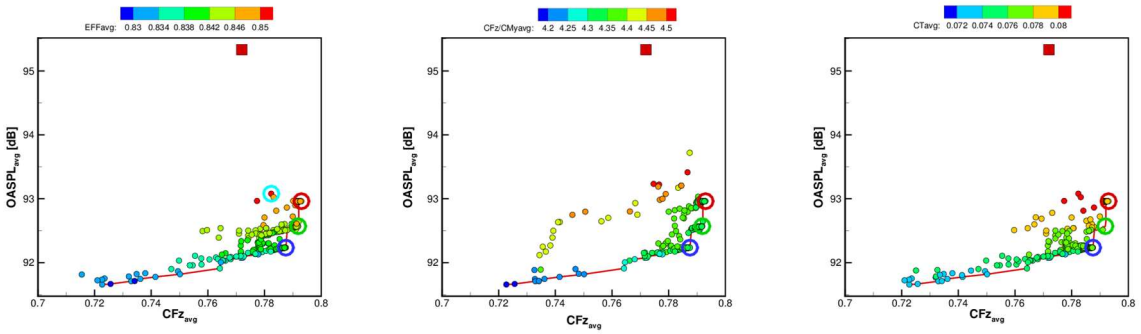

Propellers' Efficiency | Wing Lift-to-Pitching moment ratio | Pareto front: Propellers' Thrust coefficient

Figure 12: 2D and 3D Pareto fronts

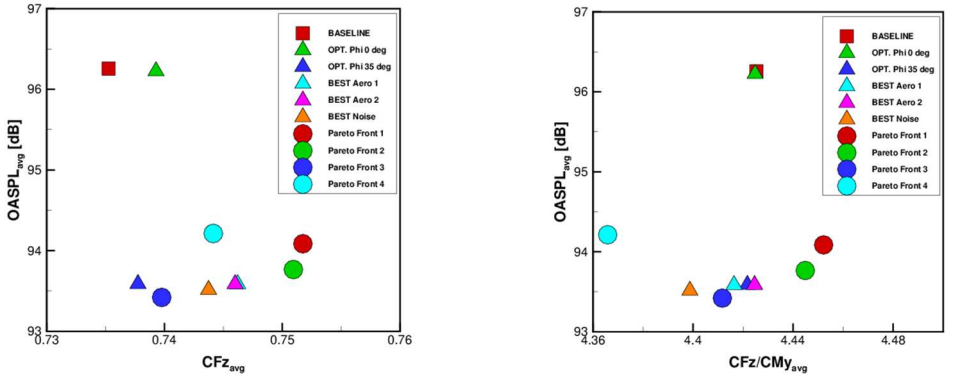

Wing Lift map | Wing Lift-to-Pitching moment ratio map

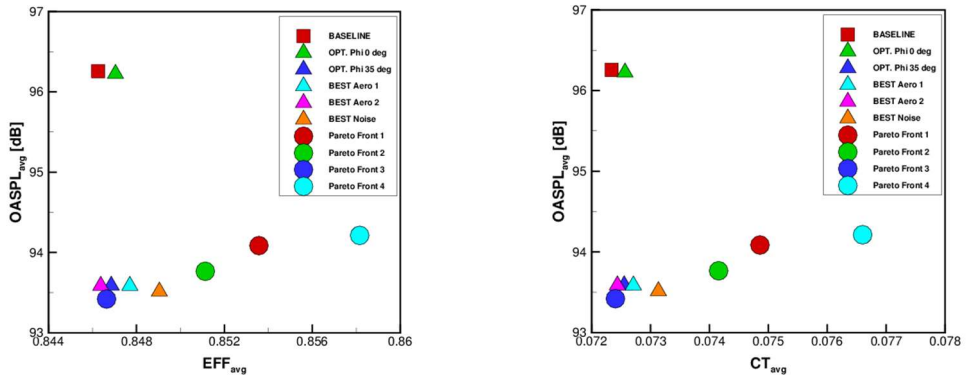

Propellers' Efficiency | Propellers' Thrust coefficient

Figure 13: Design functions results in high resolution for the representative and Pareto front points

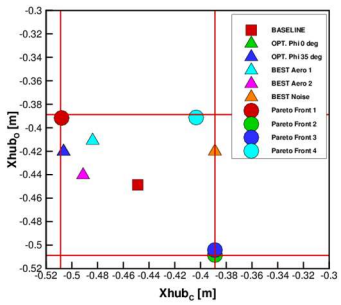

Figure 14: Map of possible chordwise (X) locations of the three propeller disk planes

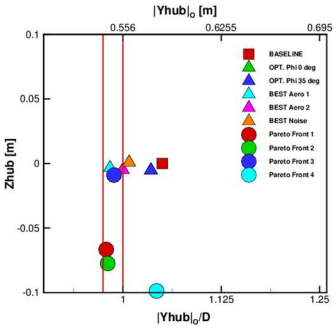

Figure 15: Map of possible spanwise (Y) and vertical locations (Z) of the three propeller disks

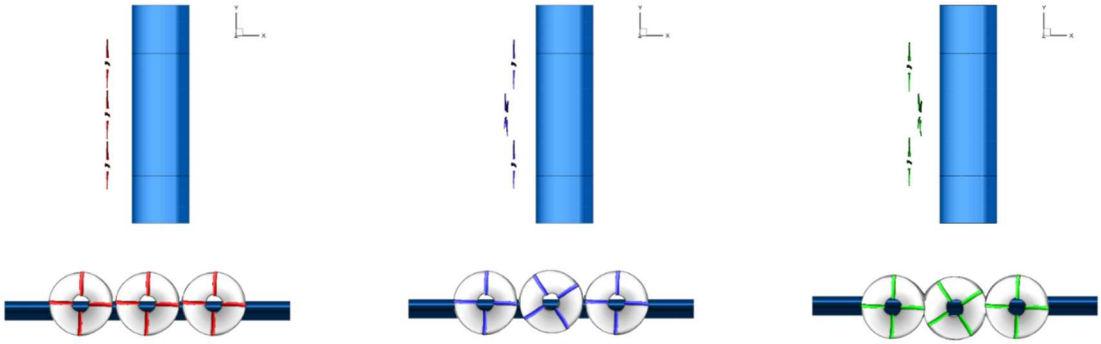

Figure 16: $OASPL_{avg}$ [dB] – Wind tunnel model layouts – Top and front view - Take-off flight condition

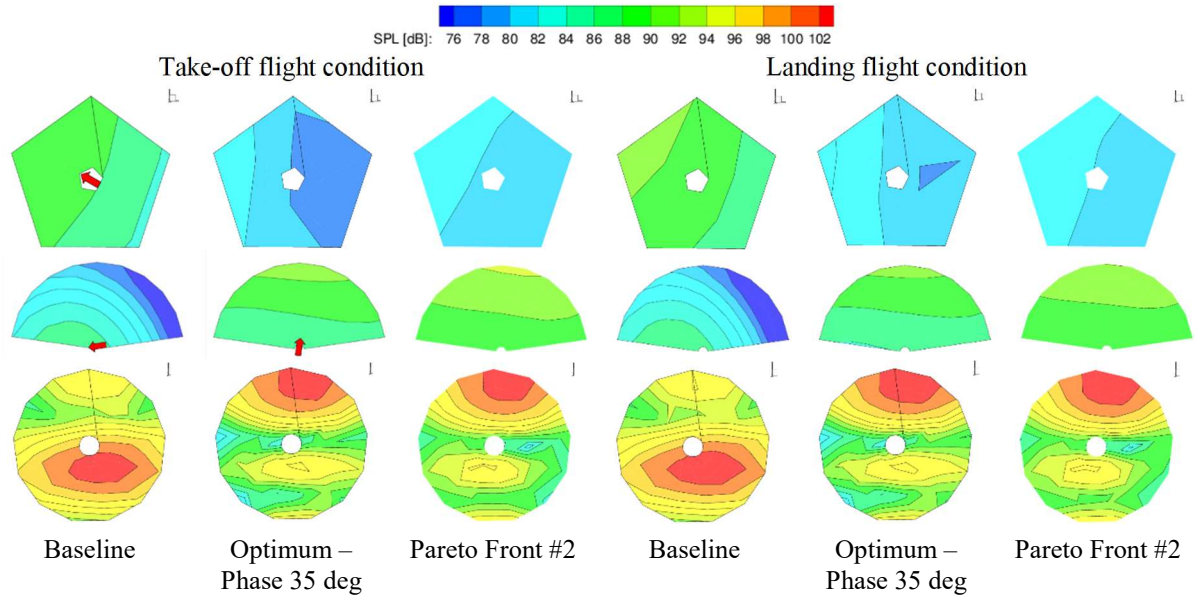

Figure 17: OASPLavg [dB] – Arrays X (top), Y (centre), Z (bottom) – Representative points